A growth interruption technique for stacking fault-free nanowire superlattices

2009 Nanotechnology 20 025610

(http://iopscience.iop.org/0957-4484/20/2/025610)

Nanotechnology **20** (2009) 025610 (6pp) doi:10.1088/0957-4484/20/2/025610

A growth interruption technique for stacking fault-free nanowire superlattices

Parsian K Mohseni and Ray R LaPierre[1]

Center for Emerging Device Technologies, Department of Engineering Physics, McMaster University, Hamilton, ON, L8S 4L7, Canada

E-mail: lapierr@mcmaster.ca

Received 5 September 2008, in final form 20 October 2008
Published 11 December 2008
Online at stacks.iop.org/Nano/20/025610

Abstract

An experimental approach to achieving phase purity in nanowires through molecular beam epitaxy growth is presented. Superlattice heterostructured nanowires were grown, consisting of alternating layers of GaAsP and GaP. The observed core–multishell heterostructure, extending axially and radially, is attributed to simultaneous Au-assisted vertical growth and diffusion-limited radial growth along lateral nanowire facets. Growth interruptions at the GaAsP/GaP interfaces allowed for the elimination of stacking faults and the growth of nanowires with a single-crystalline wurtzite phase.

(Some figures in this article are in colour only in the electronic version)

1. Introduction

Continual downscaling of optoelectronic devices can be realized through the use of low-dimensional structures as fundamental building blocks, such as semiconductor nanowires (NWs) [1]. Over the past five years, light emitting diodes (LEDs) [2], lasers [3], solar cells [4], single electron transistors [5], and optical sensors [6] have been demonstrated using NWs as the central active medium. Advances in NW research have, additionally, expanded our understanding of crystal growth and self-assembly at the nanometre scale [7, 8].

Although tremendous gains have been made towards achieving a more complete understanding of the underlying structural, electrical, and optical properties of semiconductor NWs, certain unresolved challenges remain and persistently inhibit their incorporation into mainstream device fabrication. The phase purity of NWs grown according to the vapour–liquid–solid (VLS) mechanism [9] is one such concern. In VLS growth, metal (predominantly Au) nanoparticles distributed on a substrate act as agents for the collection of gas phase adatoms. Subsequently, upon supersaturation, the metal nanoparticles act as selective-area assembly sites for nucleation and crystal growth. Such growth is achieved through various deposition methods including chemical vapour deposition (CVD) [10], metal–organic vapour phase epitaxy (MOVPE) [11], and molecular beam epitaxy (MBE) [12]. Typically, these techniques result in the formation of pseudo-one-dimensional structures with stacking faults, lamellar twins, or polytypic inclusions incorporated throughout the crystal [13, 14]. Both zincblende (Zb) and wurtzite (Wz) phases may occur in III–V semiconductor NWs as a consequence of the small difference in internal energy (<24 meV per octet pair) between the two structures [15–17]. In fact, it is a thoroughly reported observation that while certain III–V materials assume a cubic Zb structure in bulk, the preferential atomic stacking arrangement in NWs tends towards that of the hexagonal Wz arrangement [18–20]. In such systems, stacking faults, characterized as intermittent insertions of Zb in an otherwise Wz phase, can be observed [20].

As stacking faults adversely affect the fundamental material properties of NWs [21, 22], a pressing need exists for their elimination. Several successful methods for the elimination of stacking faults have been demonstrated including growth on (001) [21] or (111)A [23], as opposed to the usual (111)B, orientated substrates as well as post-growth epitaxial burying of NWs [24]. Our previous studies reported growth of stacking fault-free segments within GaP/GaAsP core–multishell NWs [20]. These segments, extending over 200 nm in length, were observed following the GaP-to-GaAsP and GaAsP-to-GaP interfaces. We now extend those previous studies by reporting the growth of stacking fault-free core–multishell superlattice (SL) heterostructured GaAsP/GaP NWs

[1] Author to whom any correspondence should be addressed.

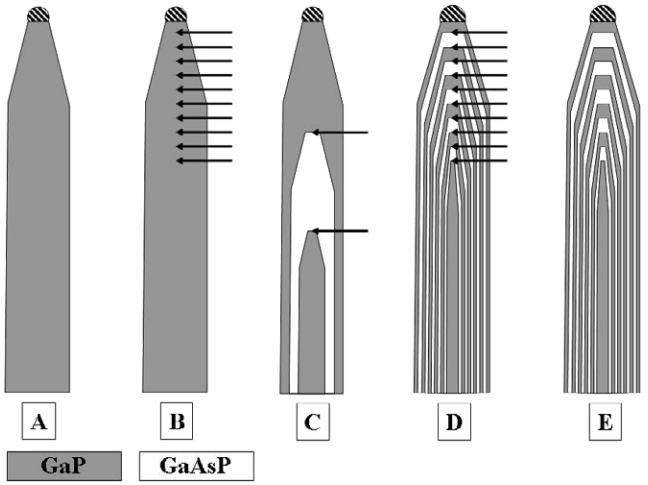

Figure 1. Pictorial representation of NW groups A–E. The shaded and white regions represent GaP and GaAsP layers, respectively, while each arrow depicts the introduction of a 3 min growth interruption. The diagonally striped regions represent the Au seeds at the NW tips. The various nanowire segments are not drawn to scale.

with a single Wz phase, achieved by a growth interruption technique.

2. Experimental details

Prior to each NW growth, a 10 Å Au film was deposited on Si(111) substrates via electron beam evaporation equipped with a quartz crystal thickness monitor. The samples were then transported in ambient air to a gas source molecular beam epitaxy system (GS-MBE). After an *in situ* inductively coupled H_2 plasma treatment at 550 °C, the Au films disseminate into uniformly distributed nanoparticles on the substrate surface. NW growth was carried out in the GS-MBE system, wherein group III monomers (Ga) were supplied from a solid elemental effusion cell and group V dimers (As_2 and P_2) were supplied from a hydride gas cracker operating at 950 °C. The growth temperature, V/III flux ratio, and nominal 2D growth rate were fixed at 510 °C, 1.5, and 1 μm h^{-1}, respectively.

Five NW groups (groups A–E) were grown via GS-MBE. The NW groups are depicted pictorially in figure 1 and summarized in table 1, together with results discussed below. Group A NWs in figure 1(a) consisted of a single GaP composition and were grown over a duration of 20 min. Group B NWs in figure 1(b), also composed of GaP grown over a total period of 20 min, were periodically subjected to 10 growth interruptions. Specifically, after the first ten minutes of growth, a 3 min interruption, wherein the shutters of the group III effusion cells were closed while maintaining a group V overpressure, was introduced followed by a 1 min growth period. This process was repeated ten times for a total growth period of 20 min. Group C NWs in figure 1(c), reported previously [20], were grown with a 3-tiered core–multishell structure. The initial layer, composed of GaP, was grown over a period of 20 min. This segment was coated with a GaAsP layer for a period of 10 min, followed by another GaP segment grown for 10 min. 3 min growth interruptions were introduced prior to the onset of each new layer. Group D NWs in figure 1(d) consisted of a GaP/GaAsP superlattice architecture, extending along the vertical and radial direction. The sample growth began with a GaP base, grown over a period of 10 min. After the initial GaP segment, 10 alternating layers of GaAsP and GaP were grown for 1 min durations with 3 min growth interruptions introduced between subsequent layers. Finally, group E NWs in figure 1(e) were grown with identical structures to those in group D but without the growth interruptions. For the sake of consistency, all GaAsP layers were grown at an As/P flux ratio corresponding to a nominal composition of $GaAs_{0.6}P_{0.4}$, as determined from previous thin film calibrations on GaAs(100) substrates. All growths were terminated by closing the shutter of the Ga cell while allowing the sample to cool under a group V overpressure.

Table 1. Sample descriptions and results amongst NW groups A–E.

NW Group	Sample description	Duration of growth interruption (min)	Density of stacking faults[a] (nm^{-1})
A	GaP (no growth interruptions)	0	0.70
B	GaP (10 growth interruptions)	3	0.40[b]
C	3-tiered GaP/GaAsP/GaP (2 growth interruptions)	3	0[b]
D	GaP/GaAsP superlattice (10 growth interruptions)	3	0[b]
E	GaP/GaAsP superlattice (no growth interruptions)	0	0.24

[a] Stacking fault densities were averaged over several NWs.
[b] Measured along NW segments grown immediately following a growth interruption.

After growth, the NWs were examined to distinguish the role of gas phase switching and growth interruptions in the formation of stacking faults. Cross-sectional analysis of as-grown NWs was conducted using a JEOL JSM-7000 scanning electron microscope (SEM) for direct comparison of NW lengths amongst different samples. The as-grown NWs were removed from the Si substrates by a 60 s ultrasonication treatment, while suspended in a small volume of de-ionized water. The suspended NWs were dispersed upon holey carbon-coated copper grids for structural and compositional analysis using a Philips CM12 transmission electron microscope (TEM) and a JEOL 2010F high resolution transmission electron microscope (HR-TEM). High angle annular dark-field (HAADF) imaging and energy dispersive x-ray spectroscopy (EDXS) was also employed in the latter instrument. For each NW group, similar results were consistently observed over a population of several dozen NWs.

3. Results and discussion

Dramatic differences in the formation of stacking faults were observed by TEM amongst the different NW groups. These results are summarized in table 1. First, GaP NWs belonging to group A exhibited a large number of densely packed faults, on the order of 0.70 nm^{-1}, distributed regularly throughout

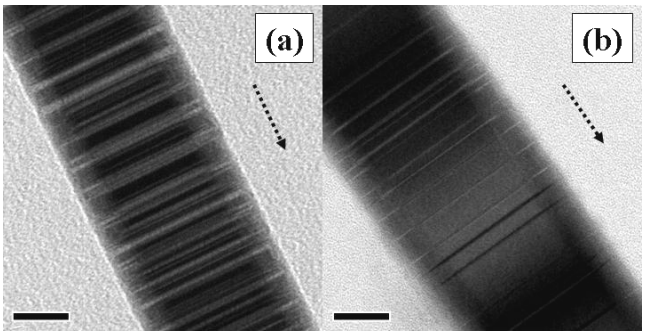

Figure 2. TEM images of single (a) group A NW and (b) group B NW. In the case of group B NWs, repeated growth interruptions were introduced, leading to the formation of fewer stacking faults. Scale bars designate a 20 nm length. Broken line indicators point toward the NW tips.

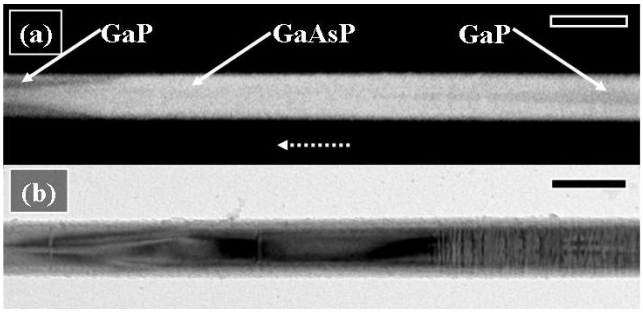

Figure 3. (a) HAADF image of a group C NW showing GaP (darker regions) and GaAsP (brighter region) segments. (b) Bright-field TEM image of corresponding region along same NW shown in (a). The formation of stacking faults is inhibited by the growth of each additional segment following a growth interruption, suggesting the potential for long range single phase crystal growth. Scale bars designate a 100 nm length. The broken line indicator points toward the NW tips.

their length, as shown in figure 2(a). Stacking faults in group B NWs, however, where periodic growth interruptions were introduced, were sparser in comparison to those in group A, at a density of roughly 0.40 nm^{-1}, as shown in figure 2(b). All values of stacking fault densities reported represent average values measured over several NWs from each sample. Hence, it would appear that growth interruptions in GaP reduced the density of stacking faults by almost a factor of two.

As previously reported [20], group C NWs were grown with a three-tiered (GaP/GaAsP/GaP) core–multishell heterostructure, as illustrated in figure 1(c). Figure 3(a) shows a HAADF image of the NW region immediately prior to, and after, the growth interruption at the first GaP/GaAsP interface. Here, contrast variations are indicative of compositional changes along the length and diameter of the NW, with bright regions corresponding to GaAsP and darker regions corresponding to GaP. A bright-field image from the identical NW region is shown in figure 3(b). Comparison with figure 3(a) reveals that the first segment (GaP core) exhibited many densely packed lateral Zb insertions. The introduction of the initial growth interruption at the GaP-to-GaAsP interface resulted in the growth of a region with no stacking fault formation. After a certain length, over 200 nm, stacking faults reformed within the GaAsP layer. A second growth interruption, introduced at the GaAsP-to-GaP interface (not shown in figure 3), then resulted in the formation of a second region along which the reformed stacking fault sequence was once again quenched. This analysis confirms the coincidence of the stacking fault elimination with the point of compositional change. As in samples A and B, the gas phase switching appeared to play an important role in the stacking fault formation.

To further examine the role of growth interruptions and material transitions on stacking faults, we turn our attention now to sample D, the superlattice sample with growth interruptions. Figure 4 shows a TEM image of a typical group D NW. Elemental counts of Ga (green), As (blue), P (red), and Au (yellow) as obtained through an EDXS linescan are superimposed on the TEM image. An axial SL heterostructure can be discerned by considering the variation in counts of P and As. At the NW base (left), the significant excess of P, in comparison to As, is indicative of a predominantly GaP base region. Moving towards the NW tip (right), the As content is observed to increase to the point where As and P counts are comparable, signifying the onset of the initial GaAsP segment. Beyond this point, the As counts are seen to decline and rise repeatedly nine times. Segments along the NW where both As and P counts are comparable

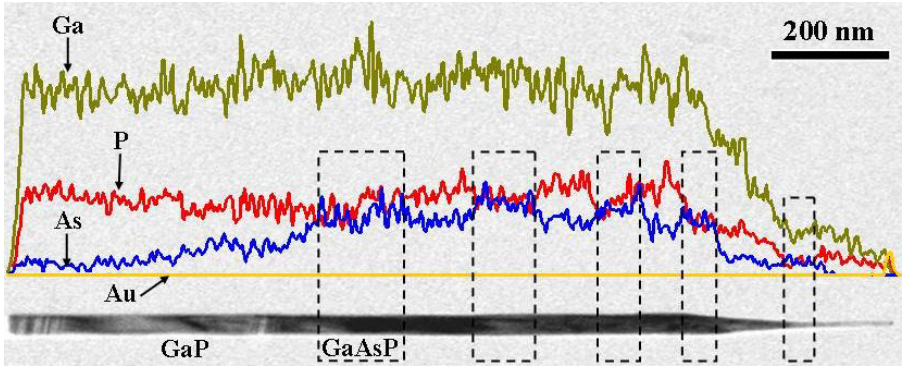

Figure 4. TEM image of single superlattice NW with superimposed EDXS linescans showing elemental counts of Ga (green), As (blue), P (red) and Au (yellow). 11 distinct segments are observed corresponding to the 11 layers within the superlattice. Segments wherein As and P counts overlap are indicative of the GaAsP layers outlined by dashed boxes, while P rich segments are characteristic of GaP layers.

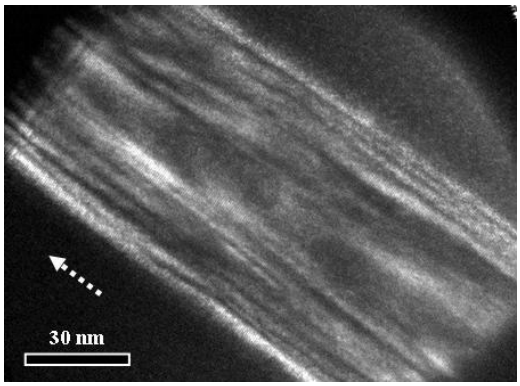

Figure 5. Dark-field TEM image obtained from the central region of a group D superlattice NW. Contrast variations across the NW width show the radially alternating layers of GaAsP (bright) and GaP (dark), confirming the core–multishell arrangement of the structure. The broken line indicator points toward the NW tip.

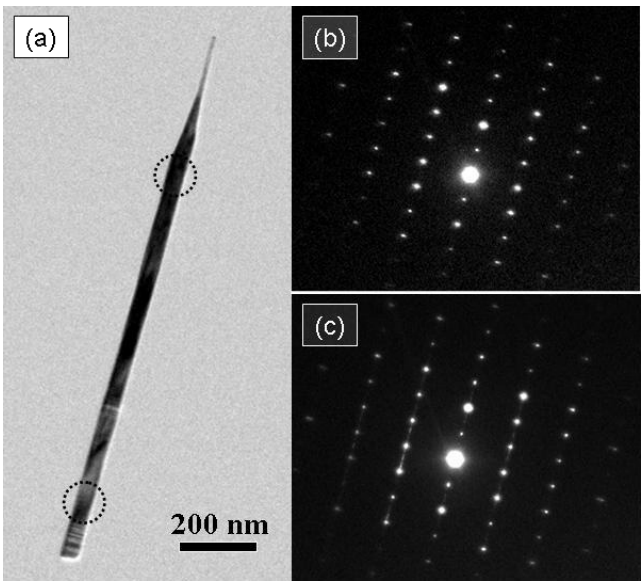

Figure 6. (a) Single NW TEM image of a group D NW. (b) SAD pattern obtained from the NW tip region (upper circled region in (a)). (c) SAD pattern obtained from the NW base (lower circled region in (a)).

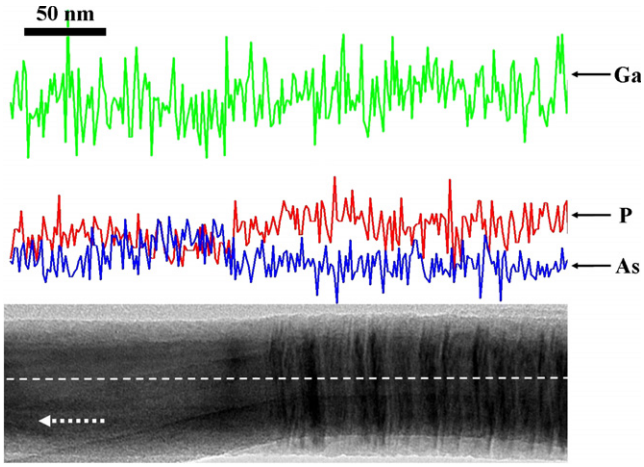

Figure 7. TEM image and superimposed EDXS counts of Ga (green), As (blue), and P (red). The termination of stacking faults in the growth direction (right to left) coincides with a region where P counts decrease as As counts increase, showing that the lateral defects are eliminated with onset of the initial GaAsP layer. The broken line indicator points toward the NW tip.

correspond to GaAsP insertions (shown as boxed regions), while P rich segments are representative of GaP insertions. Correspondingly, ten alternating segments of GaAsP and GaP are observed, indicative of the ten-tiered SL heterostructure. Each successive GaAsP layer is observed to decrease in length from the bottom to the top of the NW. This phenomenon is more pronounced towards the NW tip and can probably be attributed to the decreasing growth rate of NWs due to diffusion-limited supply of adatoms from the base, with increasing NW length.

The tapered morphology of the NW in figure 4 has previously been attributed to layer-by-layer growth based on nucleation of the diffusive adatoms on the NW sidewalls [25]. To confirm this, a HAADF image along the centre of a group D NW is shown in figure 5. Contrast variations are indicative of alternating shells of GaP (dark regions) and GaAsP (bright regions). It is evident that sidewall deposition occurs concurrently with axial VLS growth causing a radially heterostructured architecture within the SL NWs. The thickness of each shell is measured up to 5 nm. Thus, the structure of the SL NWs can be accurately described as a GaP core with 10 alternating shells of GaAsP and GaP, as depicted in figure 1(d).

TEM analysis, for example in figure 6, indicated a large number of stacking faults in the group D NWs, with densities matching those of group A, until roughly the longitudinal midpoint, where they were observed to terminate abruptly. Beyond this point, the remainder of the NWs grew in a single Wz phase, with no lateral Zb insertions, as confirmed by selective-area diffraction (SAD) analysis. The SAD pattern shown in figure 6(b), corresponding to the circled region near the top of figure 6(a), was obtained near the NW tip and is indicative of a single phase Wz crystal along the $\langle 2\bar{1}\bar{1}0\rangle$ zone axis. NW segments with lengths up to 1.2 μm were formed free of stacking faults. In contrast, the SAD pattern shown in figure 6(c), corresponding to the circled region near the bottom of figure 6(a), was obtained from a region near the NW base, where numerous densely packed stacking faults were observed. Streaking in the [0001] direction in this instance was observed, indicative of the pseudo-periodic arrangement of stacking faults in this region.

Next, the material composition of the group D NWs at the stacking fault termination point was examined. In figure 7, a TEM image near the stacking fault termination point is superimposed with EDXS linescans showing elemental counts of Ga (green), As (blue), and P (red). Moving along the growth direction (from right to left), the stacking faults cease to appear past the centre of the image. Coincident with this region, the linescan shows an increase in elemental counts of As and decrease in P, indicative of the initial GaAsP layer. Thus, the termination of stacking faults is coincident with the

initial growth interruption and the material change from GaP to GaAsP.

The length of stacking fault-free segments in group D NWs was dependent upon the diameter of the Au seeds at the NW tips. To illustrate this point, figures 8(a) and (b) show TEM images of two group D SL NWs with 14 nm and 9 nm Au diameters, respectively. The NW with the larger Au tip (a) exhibited an abrupt termination of stacking faults as described above, while the NW with the smaller Au tip (b) consisted of several segments of fault-free growth, each followed by the reappearance of Zb insertions. This effect will be elaborated further in the discussion.

Finally, group E NWs (not shown), though identical in structure to group D NWs but without growth interruptions, exhibited stacking faults throughout their lengths at a density of roughly 0.25 nm^{-1}. Cross-sectional SEM analysis revealed a mere 2% difference in lengths between group D and E NWs. This leads to the argument that the introduction of growth interruptions in group D NWs places no substantial affect upon the NW growth rate.

Theoretical considerations on the matter of Zb/Wz polytypism in thin film semiconductors have been reported in view of the compositionally variable temperature dependence [26], the scaling of structural energy difference with effective orbital ionicity [27], and the critical fractional ionic characteristic [16] of a given material. However, the case of VLS grown NWs is further complicated by the dynamic nature of the metal-semiconductor alloy employed as a physical catalyst. Akiyama *et al* [17] have shown that phase bistability in NWs relates to the ratio of the lateral facet area to the NW volume. This was shown to result in a critical diameter, dependant upon the ionicity of a material, with which both Wz and Zb layers can form. Dubrovskii *et al* [28] also have shown that the formation of polytypic arrangements in semiconductor NWs occur as a result of a surface energy decrease on the faceted sidewalls, below a material dependent critical radius. Finally, Glas *et al* [29] previously suggested that 2D nucleation occurs preferentially at the vapour–liquid–solid triple phase line where Zb forms when the supersaturation of group III (and possibly group V) adatoms is less than some critical value and conversely, that single phase Wz formation is favourable at high supersaturation. However, our recent studies [30] indicated that Wz with Zb insertions (stacking faults) occur in GaAs at high Ga or low As impingement rate, while single phase Wz occurs at low Ga or high As impingement rate. The latter results suggest the existence of some critical group III/V supersaturation below/above which a transition from polytypic growth to primarily Wz growth occurs.

In the present studies, growth interruptions were executed by shuttering the Ga source while maintaining the group V beam flux. During the growth interruption we expect the Ga to be purged from the Au particle by reaction with group V species, resulting in a low Ga supersaturation in the Au particle until growth is resumed. Compositional analysis of the Au particle, based on EDXS point measurements, revealed no significant Ga content within the seed, further substantiating the argument for the purging of group III species during growth interruptions. Consistent with the results described above for

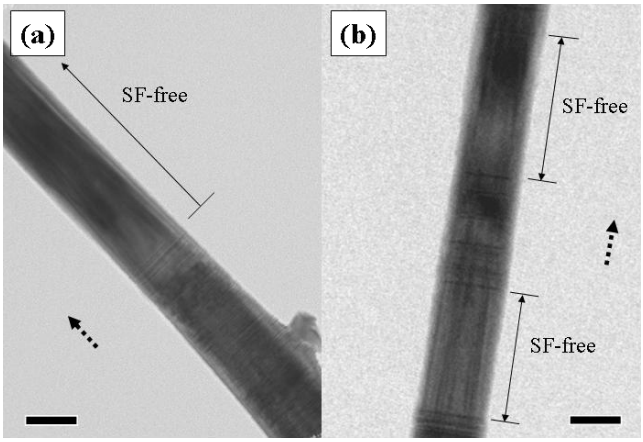

Figure 8. (a) TEM image of the stacking fault (SF) termination point within a group D NW with Au diameter of 14 nm. Beyond this point, no further stacking faults were observed. (b) TEM image of initial stacking fault termination region within a group D NW with 9 nm Au diameter. The reappearance of stacking faults shows that the suppression of Zb insertions is dependant upon the Au seed diameter and, hence, the growth rate of the NW. Scale bars designate a 50 nm length. The broken line indicators point toward the NW tips.

GaAs growth, we speculate that once growth is resumed, a transient period occurs where the group III supersaturation is below some critical concentration favouring fault-free Wz NW segments. As growth proceeds, increasing Ga supersaturation returns the nanowire to a polytypic Wz/Zb phase. With respect to homoepitaxially grown GaAs NWs, it has been reported that under conditions similar to the growth interruptions discussed here, where group V pressures are maintained in the absence of group III pressures, a 'cooling necking' occurs leading to a characteristic narrow tip of dissimilar phase [29, 30]. Such an effect was not observed amongst any of the NWs investigated in the current study. The basis for the absence of a visible neck formation after growth interruptions in our heteroepitaxially grown GaAsP/GaP systems remains a topic of further examination.

The diameter dependence of stacking faults discussed with regards to figure 6 can be attributed to the dependence of growth rate upon seed diameter. NW growth rates are inversely proportional to the diameters of the Au particles at their tips [31, 32]. Thus, it is expected that in faster growing NWs with smaller particles, growth interruptions are not introduced at sufficiently high frequencies, thereby allowing for the reformation of stacking faults in each segment as steady-state concentrations are established in the Au particles. From these results, we can conclude that if growth interruptions are repeatedly introduced between sufficiently short NW segments, then the reappearance of stacking faults can be suppressed and phase purity can be sustained over the entire length of a NW.

4. Conclusions

In summary, growth of stacking fault-free superlattice heterostructured NWs has been demonstrated via Au-assisted GS-MBE. Growth interruptions at the heterostructure

interfaces permit the formation of single phase Wz segments. Thus, control over the compositionally dynamic Au-based alloy can be gained to allow for single phase NW growth.

Acknowledgments

We gratefully acknowledge the financial support of the Natural Sciences and Engineering Research Council (NSERC) of Canada and the Ontario Centres of Excellence. Additionally, we thank Brad Robinson for MBE growths and Fred Pearson for HR-TEM assistance.

References

[1] Semiconductor Industry Association 2007 *The International Technology Roadmap for Semiconductors*
[2] Svensson C P T, Martensson T, Tragardh J, Larsson C, Rask M, Hessman D, Samuelson L and Ohlsson J 2008 *Nanotechnology* **19** 305201
[3] Agarwal R, Barrelet C J and Lieber C M 2005 *Nano Lett.* **5** 917
[4] Tian B, Zheng X, Kempa T J, Fang Y, Yu N, Yu G, Huang J and Lieber C M 2007 *Nature* **449** 885
[5] Thelander C, Martensson T, Bjork M T, Ohlsson B J, Larsson M W, Wallenberg L R and Samuelson L 2003 *Appl. Phys. Lett.* **83** 2052
[6] Mu L, Shi W, Chang J C and Lee S-T 2008 *Nano Lett.* **8** 104
[7] Borgstrom M T, Immink G, Ketelaars B, Algra R and Bakkers E P A M 2007 *Nat. Nanotechnol.* **2** 541
[8] Harmand J C, Tchernycheva M, Patriarche G, Travers L, Glas F and Cirlin G 2007 *J. Cryst. Growth* **301** 853
[9] Wagner R S and Ellis W C 1964 *Appl. Phys. Lett.* **4** 89
[10] Lauhon L J, Gudiksen M S, Wang D and Lieber C M 2002 *Nature* **420** 57
[11] Seifert W *et al* 2004 *J. Cryst. Growth* **272** 211
[12] Chen C, Braidy N, Couteau C, Fradin C, Weihs G and LaPierre R R 2008 *Nano Lett.* **8** 495
[13] Joyce H J, Gao Q, Tan H H, Jagadish C, Kim Y, Zhang X, Guo Y and Zou J 2007 *Nano Lett.* **7** 921
[14] Karlsson L S, Dick K A, Wagner J B, Malm J-O, Deppert K, Samuelson L and Wallenberg L R 2007 *Nanotechnology* **18** 485717
[15] Yeh C-Y, Lu Z W, Froyen S and Zunger A 1992 *Phys. Rev.* B **46** 10086
[16] Ito T 1998 *Japan. J. Appl. Phys.* **37** L1217
[17] Akiyama T, Sano K, Nakamura K and Ito T 2006 *Japan. J. Appl. Phys.* **45** L275
[18] Persson A I, Larsson M W, Stenstrom S, Ohlsson B J, Samuelson L and Wallenberg L R 2004 *Nat. Mater.* **3** 677
[19] Ihn S-G, Song J-I, Kim T-W, Leem D-S, Lee T, Lee S-G, Koh E K and Song K 2007 *Nano Lett.* **7** 39
[20] Mohseni P K, Maunders C, Botton G A and LaPierre R R 2007 *Nanotechnology* **18** 445304
[21] Krishnamachari U, Borgstrom M, Ohlsson B J, Panev N, Samuelson L, Seifert W, Larsson M W and Wallenberg L R 2004 *Appl. Phys. Lett.* **85** 2077
[22] Bao J, Bell D C, Capasso F and Wagner J B 2008 *Nano Lett.* **8** 836
[23] Wacaser B A, Deppert K, Karlsson L S, Samuelson L and Seifert W 2006 *J. Cryst. Growth* **287** 504
[24] Patriarche G, Glas F, Tchernycheva M, Sartel C, Largeau L and Harmand J-C 2008 *Nano Lett.* **8** 1638
[25] Chen C, Plante M C, Fradin C and LaPierre R R 2006 *J. Mater. Res.* **21** 2801
[26] Kulakov M P and Balyakina I V 1991 *J. Cryst. Growth* **113** 653
[27] Yeh C-Y, Lu Z W, Froyen S and Zunger A 1992 *Phys. Rev.* B **45** 12130
[28] Dubrovskii V G and Sibirev N V 2008 *Phys. Rev.* B **77** 035414
[29] Glas F, Harmand J-C and Patriarche G 2007 *Phys. Rev. Lett.* **99** 146101
[30] Plante M C and LaPierre R R 2008 *Nanotechnology* at press
[31] Plante M C and LaPierre R R 2006 *J. Cryst. Growth* **286** 394
[32] Dubrovskii V G, Sibirev N V, Cirlin G E, Harmand J-C and Ustinov V M 2006 *Phys. Rev.* E **73** 021603